Applied Thermal Engineering 123 (2017) 61–73

Contents lists available at ScienceDirect

Applied Thermal Engineering

journal homepage: www.elsevier.com/locate/apthermeng

Research Paper

Influence of geometric characteristics of a diesel particulate filter on its behavior in equilibrium state

Yuanwang Deng [a,b,d], Wenping Zheng [a,b], Jiaqiang E [a,b,d,*], Bin Zhang [a,b], Xiaohuan Zhao [a,b], Qingsong Zuo [c], Zhiqing Zhang [a,b], Dandan Han [a,b]

[a] State Key Laboratory of Advanced Design and Manufacturing for Vehicle Body, Hunan University, Changsha 410082, China
[b] College of Mechanical and Vehicle Engineering, Hunan University, Changsha 410082, China
[c] College of Mechanical Engineering, Xiangtan University, Xiangtan 411105, China
[d] Institute of New Energy and Energy-Saving & Emission-Reduction Technology, Hunan University, Changsha 410082, China

HIGHLIGHTS

- A pressure drop model of the DPF in equilibrium state is developed.
- Effects of key factors on equilibrium properties of the DPF are investigated.
- Impacts of five factors on equilibrium properties of the DPF are evaluated.
- Larger wall thickness and smaller channel diameter cause more soot mass in the DPF in equilibrium state.
- Depending on diameter of the filter, the optimum length of the filter may not necessarily be the smallest possible.

GRAPHICAL ABSTRACT

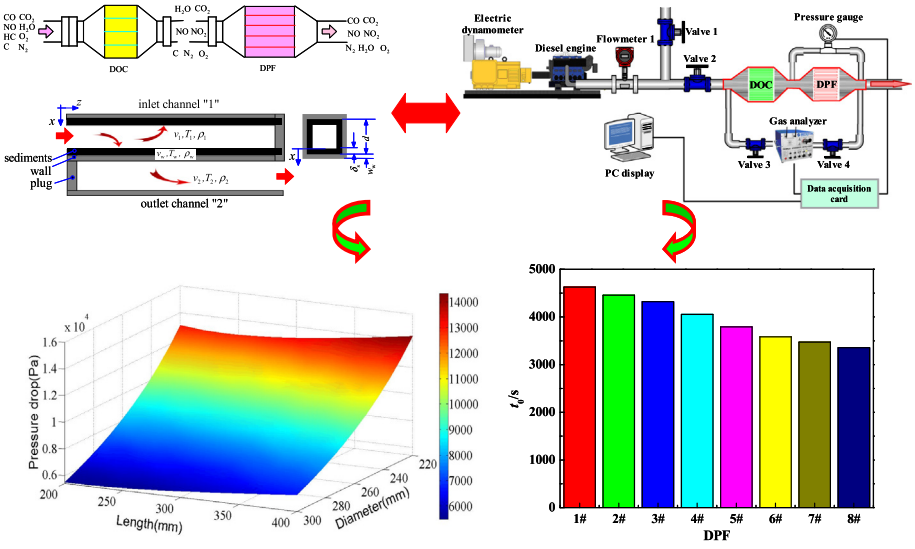

ARTICLE INFO

Article history:
Received 11 December 2016
Revised 11 April 2017
Accepted 13 May 2017
Available online 18 May 2017

Keywords:
Continuous regeneration technology
Equilibrium characteristics
Weighting factors

ABSTRACT

In order to enhance behaviors of the diesel particulate filter (DPF) in equilibrium state, a mathematic model of pressure drop in the DPF in equilibrium state is developed to investigate effects of key parameters on its behavior in equilibrium state. Therefore, the impacts of factors on soot mass in the DPF in equilibrium state, pressure drop in the DPF in equilibrium state and oxidation rate are evaluated by the improved fuzzy grey relational analysis method. And some useful results such as fuzzy grey correlation coefficient of different effect factors in equilibrium state of the diesel particulate filter in the process of continuous regeneration and change laws of soot mass and pressure drop in the DPF in equilibrium state based on different geometric parameters are obtained. Smaller diameter of the DPF will result in larger pressure drop in the DPF and more complications for the length of the filter in equilibrium state.

* Corresponding author at: State Key Laboratory of Advanced Design and Manufacturing for Vehicle Body, Hunan University, Changsha 410082, China.
E-mail address: ejiaqiang@126.com (J. E).

http://dx.doi.org/10.1016/j.applthermaleng.2017.05.071

Diesel particulate filter
Aftertreatment technique

The optimum length of the filter may not necessarily be the smallest possible, sometimes depending on diameter of the filter in equilibrium state. Larger wall thickness and smaller channel diameter cause more soot mass in the DPF in equilibrium state. This work will provide relative reference values when the diesel particulate filter is chosen or designed to match the CRT system.

Nomenclature

c_m	general migration constant;
$c_{p,s}$	specific heat capacity of particles layer (J kg^{-1} K^{-1})
$c_{p,w}$	specific heat capacity of wall (J kg^{-1} K^{-1})
d	channel diameter of the filter (μm)
D	diameter of the diesel particulate filter (DPF) (mm)
E_1	activation energy of soot oxidized by O_2 into CO (J/K)
E_2	activation energy of soot oxidized by O_2 into CO_2 (J/K)
E_3	activation energy of soot oxidized by NO_2 into CO (J/K)
E_4	activation energy of soot oxidized by NO_2 into CO_2 (J/K)
E_5	activation energy of soot oxidized by NO_2 into CO_2 (J/K)
E_6	activation energy of soot oxidized by NO_2 into CO (J/K)
E_f	activation energy in the CO/CO_2 shift reaction (J/K)
f_{CO}	selectivity of thermal regeneration
F	pressure drop coefficient of square hole
m	total number of factors
m_q	soot mass concentration (g L^{-1})
m_s	local mass of soot (kg)
M_1	molar mass of O_2 (mol kg^{-1})
M_2	molar mass of NO_2 (mol kg^{-1})
L	length of the filter (m)
$n_{channel}$	channel number of DPF
p_0	atmospheric pressure (Pa)
p_1	pressure of gas flow in channel 1 (Pa)
p_2	pressure of gas flow in channel 2 (Pa)
k_1	reaction rate constant (L K^{-1} s^{-1}), $k_1 = 5 \times 10^8$ L K^{-1} s^{-1}
k_2	reaction rate constant (L K^{-1} s^{-1}), $k_2 = 5 \times 10^8$ L K^{-1} s^{-1}
k_3	reaction rate constant (L s^{-1}), k_3 = 10,000 L s^{-1}
k_4	reaction rate constant (L s^{-1}), k_4 = 10,000 L s^{-1}
k_5	reaction rate constant (L s^{-1})
k_6	reaction rate constant (L s^{-1})
k_f	frequency factor in the CO/CO_2 shift reaction
k_s	permeability of soot particles layer (m^2), $k_s = 7 \times 10^{-14}$ - m^2
k_w	permeability of wall (m^2), $k_w = 1 \times 10^{-12}$ m^2
r_{ij}	fuzzy grey correlation coefficient
R	molar gas constant (J K^{-1} mol^{-1}), R = 8.314 J K^{-1} mol^{-1}
$r_{1\text{-}ij}$	cosine value of fuzzy factors
$r_{2\text{-}ij}$	Euclidean coefficient
$X(X')$	matrix of comparison factors
Y	matrix of reference targets
x_i (x'_i)	comparison factors
y_i	comparison factors
l	resolution coefficient, l ∈ [0,1]
R_i	reaction rate of main reactions, i = 1, 2, 3, 4, 5, 6
T_0	initial temperature of inlet gas (K)
T_1	temperature of the exhaust gas in the inlet (K)
T_s	solid temperature of the porous medium
T_2	temperature of the exhaust gas in the outlet (K)
T_w	temperature of exhaust gas inside the filter (K)
v_0	initial temperature of inlet gas (Pa)
v_1	velocity of gas flow in channel 1 (m s^{-1})
v_2	velocity of gas flow in channel 2 (m s^{-1})
v_w	velocity of gas flow inside the filter (m s^{-1})
$v_{wall,1}$	wall velocity in the inlet channel (m s^{-1})
$v_{wall,2}$	wall velocity in the outlet channel (m s^{-1})
w_w	wall thickness of the filter (mm)
δ_0	local deposited soot height (m)
δ_s	thickness of particles layer (m)
δ_{sc}	local deposited soot height (m)
λ_s	thermal conductivity of particles layer (W m^{-1} K^{-1})
λ_w	thermal conductivity of the filter (W m^{-1} K^{-1})
ΔH_1	reaction enthalpy between soot and O_2 (J)
ΔH_2	reaction enthalpy between soot and NO_2 (J)
Δp	pressure drop of the DPF (Pa)
Δm_q	soot mass in the DPF under equilibrium state (g)
Δz_{cell}	length of computational cell in axial direction
ρ_1	density of gas flow in channel 1 (kg m^{-3})
ρ_2	density of gas flow in channel 2 (kg m^{-3})
ρ_s	density of particles layer (kg m^{-3})
ρ_w	density of exhaust gas inside the filter (kg m^{-3})
μ	exhaust gas viscosity (Pa s)
ξ_{in}	pressure loss coefficient of inlet
ξ_{out}	pressure loss coefficient of outlet
α_1	selectivity coefficient for completely reaction between O_2 and carbon particle, with a range from 0.55 to 0.9
α_2	selectivity coefficient for completely reaction between NO_2 and carbon particle, with a range from 1.2 to 1.8

1. Introduction

With the rapid increase of vehicle ownership, environmental pollution of vehicles has become a worldwide problem [1,2]. Currently, there has been a great efforts with a numerous research papers in some new combustion modes (Partially Premixed Compression Ignition (PPCI) [3,4], RCCI (Reactivity Controlled Compression Ignition) [5–8], HCCI (Homogeneous Charge Compression Ignition) [9,10], etc. [11–14]) that solve the particulate emissions from the diesel engine, and the diesel particulate filter (DPF) technology is considered to be one of the most effective and simplest method to reduce particulate emission [15,16] and its regeneration technology [17,18] is the key factor for actual application of the DPF.

Various schemes are being considered by engine manufacturers for DPFs regeneration, such as microwave heating, catalytic regeneration, etc [19,20]. It is worth noting that microwave heating is considered promising and particularly suitable for soot combustion in a SiC DPF, with significantly lower soot ignition temperatures due to the instantaneous penetration of microwaves into the filter body and the selective absorption of microwaves by the soot layer [21], therefore, SiC DPFs regeneration by means of microwaves applications has been successfully applied [22,23], and the effective regeneration effects have been receiving widespread attention. Among many aftertreatment technologies for reducing particulate emission, the continuous regeneration technology (CRT) [24,25], the main protagonist, has many merits, including regeneration at normal temperature as low as 250 °C,

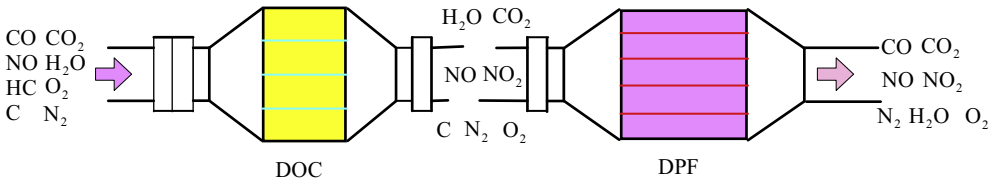

Fig. 1. Work process of the CRT.

and no additional energy [26,27], which make it a promising way in the aftertreatment of diesel engine [28–31]. It has a more simple working process shown in Fig. 1. Firstly, rather low NO_2 concentrations with 5–15% of total NO_x is increasing by the diesel oxidation catalyst (DOC) effectively with the NO_2 concentrations to 50% of NO_x by oxidizing the NO in the exhaust stream and the upstream temperature of diesel particulate filter is increasing slightly by converting HC and CO [32,33]. Then, sufficient NO_2 is capable of consuming soot along with the participation of O_2. Finally, a small amount of existing soot is acquired in the filter when regeneration reaches a certain degree to reduce the exhaust back pressure and to make sure that engines operate in high performance [34,35]. In the final results of regeneration process, the equilibrium properties of regeneration of filters should be attached to great importance, which has a significantly impact on engine performance and aftertreatment optimization.

As it is well known that equilibrium characteristics of regeneration of filters, a dynamic balance with characteristic of subtle variation of soot mass and pressure drop, where the particle loading rate equals to the consuming rate, are easily affected to many factors, and many investigations and experiments are conducted [36,37]. Kandylas and Koltsakis [38] researched equilibrium characteristics with the illustrative model corresponding to various operating conditions in ESC test cycle, regarding variation of particle deposition mass as main index to study the CRT behavior. The results showed that mass ratio with NOx/soot is no less than 7.2 and the temperature should be greater than 250 °C. Konstandopoulos [39] partly mentioned the relations between pressure drops and channels per square inch (CPSI). Tang et al. [40] investigated the filtration and continuous regeneration of a diesel particulate filter system on an engine test bench including a diesel oxidation catalyst (DOC) and a catalyzed diesel particulate filter (CDPF) and provides a method for determining the balance point temperature by measuring the trend of solid particle number concentration. Bai et al. [41] established a new soot estimation model to calculate the soot accumulation with soot maintaining around 1.27 g/L when temperature reaches 283 °C and NO_2 concentration keeps 289 ppm at balance point. A mathematic model of the NO_2-assisted regeneration is developed by E et al. [25] to study the effects from exhaust airflow to filter structure on regeneration speed in NO_2-assisted regeneration process.

To sum up, it can be seen that the equilibrium characteristics of regeneration is divided into two categories [24]. One category is critical state whether the regeneration of filters works normally to make sure minimum requirements of normal operation, and the other is equilibrium state where the oxidation rate decreases gradually on the basis of Arrhenius equation, and finally in accordance with particle loading rate during normal regeneration. Two indexes such as pressure drop and soot mass are relatively fatal on equilibrium characteristics of the CRT. Since exhaust back pressure has a direct influence on comprehensive performance of the engine and excess soot mass in the DPF in equilibrium state will cause some bad influences such as soot substances forming easily into lumps, their oxidation being more difficult, channels being easily plugged and finally will lead to the regeneration of the DPF being deteriorated [42–44].

In order to improve the dynamic equilibrium characteristics of the CRT, how to find out some laws that can make equilibrium state of regeneration for the CRT be lower pressure and lower soot mass is very important for the aftertreatment technology. Different from previous works, in this paper, the authors mainly investigate the effect of geometric parameters of the DPF on equilibrium state of the CRT, where the pressure drop in the DPF in equilibrium state is largely concentrated on, pursuing to find out the primary factor influencing soot mass in the DPF in equilibrium state, pressure drop in the DPF in equilibrium state. Besides, the oxidation rate of soot was taken into considered. This work will provide relative reference values when the diesel particulate filter is chosen or designed to match the CRT system.

2. Mathematic model and variation

As mentioned, the effects of the DPF on equilibrium characteristics are investigated with little oxidation catalyst, getting by measuring exhaust composition of the DPF entrance in steady state as the inlet conditions of regeneration model.

2.1. Diesel particulate filter model

This model is established on the basis of previously typical researches [45–47] and Ref. [8], and some assumptions are considered: (a) Soots are consisted of solid particles and void space; (b) The void space is randomly distributed and is reasonably uniform in size; (c) No void space is sealed off; (d) There are no diffusion phenomena and no ash; (e) The height of soot layer is considered.

The model of single channel is showed in Fig. 2. As shown in Fig. 2, the exhaust gas going through the DOC flows into an inlet

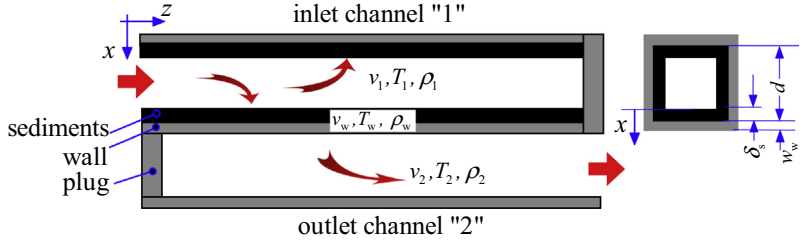

Fig. 2. Flow model of a filter channel consisted of inlet and outlet channel.

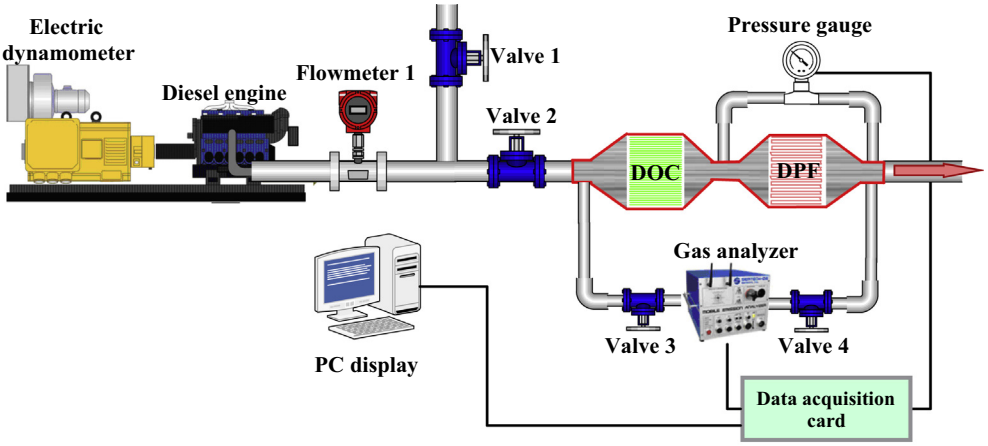

(a) Schematic diagram of the test bench

(b) Main equipments in the test bench

Fig. 3. Test system of the continuous regeneration of the DPFs.

Table 1
Technical parameters of the diesel engineYC4A.

SN	Parameter	Value
1	Cylinder number	4
2	Compression ratio ε	17.5
3	Air induction	Turbocharged/after cooling
4	Displacement V/L	4.84
5	Max velocity n/r min^{-1}	2300
6	Max power P_{max}/kW	85
7	Max peak torque T/N m	450

Table 2
Main parameters of the DOC.

Parameter	Value
Diameter (mm)	266
Length (mm)	150
Channel wall thickness (mm)	0.19
Wall pore diameter (μm)	49.1
Channel width (mm)	1.5
Washcoat loading (Pt) (g/L)	1.8

channel and is expelled out from an outlet of the DPF, the particulate is deposited on the inside channel wall or gradually oxidized by O_2 and NO_2. As a result, the governing equations of gas are given as bellow:

Applying continuity to the wall flux through the soot layer leads to an expressing:

$$v_{wall}(x) = v_{wall,1}\frac{\rho_1(d-2\delta_s)}{d-2\delta_s+2x} \quad (1)$$

Table 3
Initial parameters for the experimental verification.

Parameters	Value
Engine speed/rpm	2000
Engine load/%	20.0
Exhaust gas recycling rate/%	15
Injection pressure (MPa)	65
Exhaust temperature (K)	545
Exhaust flow rate (kg s^{-1})	0.40
Volume fraction of the $NO_2/10^{-6}$	300
$m(NO_2)/m$(soot) in gas	21
Volume fraction of the O_2/%	20

$$v_{wall,2} = v_{wall,1}\frac{\rho_1(d-2\delta_s)}{\rho_2 d} \tag{2}$$

And the Eq. (2) is inserted into mass equation, so conservation of mass equation can be expressed as follows:

$$\frac{\partial \rho_1 v_1^2 (d-2\delta_s)^2}{\partial z} = -4(d-2\delta_s)\rho_1 v_{wall,1} \tag{3}$$

$$d^2\frac{\partial \rho_2 v_2^2}{\partial z} = 4d\rho_1 v_{wall,1}(d-2\delta_s) \tag{4}$$

For conservation of momentum equation:

$$\frac{\partial \rho_1 v_1^2 (d-2\delta_s)^2}{\partial z} = -4(d-2\delta_s)\rho_1\frac{\partial p_1}{\partial z} - F\mu v_1 \tag{5}$$

$$d^2\frac{\partial \rho_2 v_2^2}{\partial z} = d^2\frac{\partial p_2}{\partial z} - F\mu v_2 \tag{6}$$

The main regeneration reaction of the DPF can be described as follows [48–51].

$$C + 1/2O_2 \xrightarrow{k_1} CO \tag{7}$$

$$C + O_2 \xrightarrow{k_2} CO_2 \tag{8}$$

$$C + NO_2 \xrightarrow{k_3} CO + NO \tag{9}$$

$$C + 2NO_2 \xrightarrow{k_4} CO_2 2NO \tag{10}$$

$$C + NO_2 + 1/2O_2 \xrightarrow{k_5} CO_2 NO \tag{11}$$

$$C + NO_2 + 1/2O_2 \xrightarrow{k_5} CONO_2. \tag{12}$$

Based on Ref. [52–54], the common rates accord with Arrhenius-type functions can be revised as follows:

$$R_1 = f_{CO}k_1 T_s y_{O_2}\exp\left(\frac{-E_1}{RT_s}\right) \tag{13}$$

$$R_2 = (1-f_{CO})k_2 T_s y_{O_2}\exp\left(\frac{-E_2}{RT_s}\right) \tag{14}$$

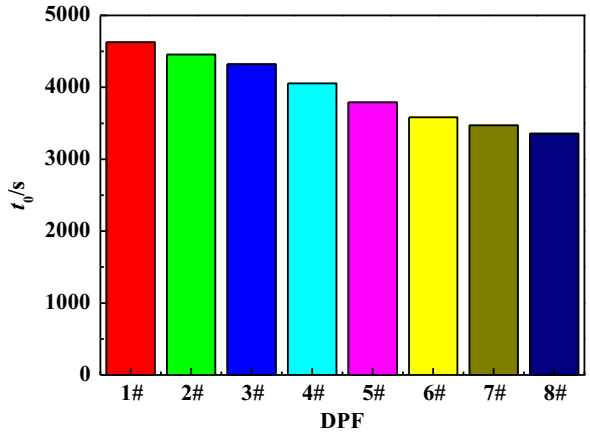

Fig. 4. Measurement value of regeneration time.

Table 5
Test validation of the DPFs.

–	Capture time (s)	Maximal relative error of pressure drop (%)	Maximal relative error of mass (%)
1#DPF	4626	1.7442	2.7650
2#DPF	4457	1.8935	2.9379
3#DPF	4321	2.2892	3.7240
4#DPF	4054	2.2086	3.3970
5#DPF	3792	2.3457	3.4152
6#DPF	3584	2.2642	2.9713
7#DPF	3472	2.3077	4.1941
8#DPF	3357	2.4675	3.1915

$$R_3 = f_{CO}k_3 y_{NO_2}\exp\left(\frac{-E_3}{RT_s}\right) \tag{15}$$

$$R_4 = (1-f_{CO})k_4 y_{NO_2}\exp\left(\frac{-E_4}{RT_s}\right) \tag{16}$$

$$R_5 = f_{CO}k_5 y_{NO_2} y_{O_2}\exp\left(\frac{-E_5}{RT_s}\right) \tag{17}$$

$$R_6 = (1-f_{CO})k_6 y_{NO_2} y_{O_2}\exp\left(\frac{-E_6}{RT_s}\right) \tag{18}$$

where the f_{CO} can be calculated by Eq. (19) [38].

$$f_{CO} = \frac{1}{1+k_f y_{NO_2}\exp\left(\frac{-E_f}{RT_s}\right)} \tag{19}$$

The energy balance of solid phase, i.e. carbon particles, should be taken into account:

Table 4
Test matrix of the DPFs.

Key parameters	1#DPF	2#DPF	3#DPF	4#DPF	5#DPF	6#DPF	7#DPF	8#DPF
L/mm	250	300	350	400	250	300	350	400
d/μm	75	58	48	38	75	58	48	38
w_w/mm	0.21	0.31	0.41	0.51	0.21	0.31	0.41	0.51
D/mm	220	266	300	300	220	220	266	300
λ_w/W m^{-1} K^{-1}	1.6	1.6	1.6	1.6	15	15	15	15

$$\frac{\partial T_w}{\partial t}\left(\delta_s\rho_s c_{p,s}+\rho_w w_w c_{p,w}\right)=h_1(T_1-T_w)+h_2(T_2-T_w)+\rho_w v_w c_{p,w}(T_1-T_w)+\frac{\Delta H_1}{M_1}[\alpha_1 R_1+(1-\alpha_1)R_2]+\frac{\Delta H_2}{M_2}[\alpha_2 R_3+(2-\alpha_2)R_4]-\lambda_s\frac{\partial}{\partial z}\left(\delta_s\frac{\partial T_w}{\partial z}\right)+\lambda_w\frac{\partial}{\partial z}\left(w_w\frac{\partial^2 T_w}{\partial^{2z}}\right) \quad (20)$$

where initial boundary conditions are confirmed by Eq. (21).

$$\begin{cases} t=0, z=0: v_1=v_0, \delta_s=\delta_0, T_1=T_0 \\ z=L: v_2=0, p_2=p_0, T_2=T_w \end{cases} \quad (21)$$

During the regeneration process, we consider the soot migration interacted between flow and soot particles to be transported along the channel and causing redistribution of soot, and it depends on local deposited soot height and the inlet channel velocity, then it can be expressed by

$$\frac{\partial \delta_s}{\partial t}+c_m\frac{\partial(v_1\delta_s)}{\partial z}=0 \quad (22)$$

where boundary conditions are applied:

$$t=0, z=0: v_1=v_0, \delta_s=\delta_0 \quad (23)$$

And the local height of the soot layer can be derived from the soot mass and there is a soot balance, showed in the following:

$$\delta_s=\frac{1}{2}d-\sqrt{d^2-\frac{m_s}{n_{channel}\Delta z_{cell}\rho_s}} \quad (24)$$

Besides, the pressure drop in the DPF in equilibrium state can be separated into four parts that is developed by software AVL Fire v2013, including flow resistance passing through the soot cake and wall, and pressure drop loss of the inlet and outlet. The pressure drop in the DPF in equilibrium state can be calculated as follows:

$$\Delta p=\frac{\mu}{k_s}\int_{x=0}^{x=\delta_s} v_{wall}(y)dy+\frac{\mu w_w}{k_w}v_{wall,2}+\xi_{in}\frac{\rho_1 v_1^2}{2}+\xi_{out}\frac{\rho_2 v_2^2}{2} \quad (25)$$

According to the Eq. (24), (25), pressure drop Δp in the DPF in equilibrium state is finally expressed by Eq. (26).

$$\Delta p=\frac{\mu}{2k_s}(d-2\delta_s)v_{wall,1}\ln\frac{d}{d-2\delta_s}+\frac{\mu w_w}{k_w}v_{wall,1}\frac{p_1 T_w}{p_2 T_1}\cdot\frac{(d-2\delta_s)}{d}+\xi_{in}\frac{\rho_1 v_1^2}{2}+\xi_{out}\frac{\rho_2 v_2^2}{2} \quad (26)$$

According to the previous studies [55–58] and Eq. (26), it is concluded that pressure drop Δp in the DPF in equilibrium state is a function including five factors such as channel diameter d of the filter, wall thickness w_w of the filter, length L of the filter, diameter D of the DPF and thermal conductivity λ_w of the filter.

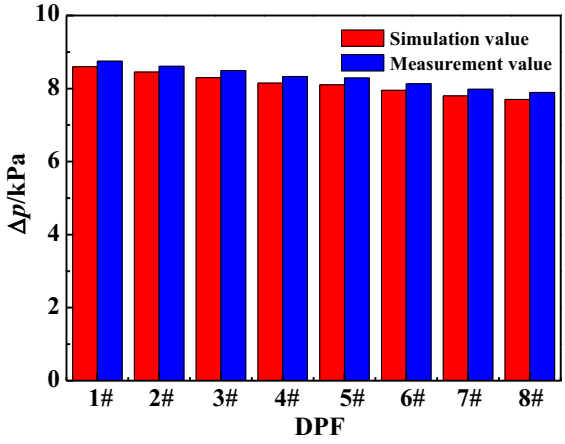

(a) Pressure drop at the end of soot capture process

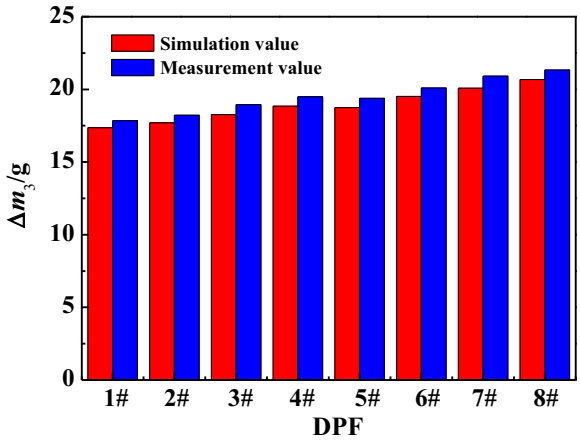

(b) Mass Δm_3 of the captured soot at the end of soot capture process

Fig. 5. Comparison between experiment and simulation.

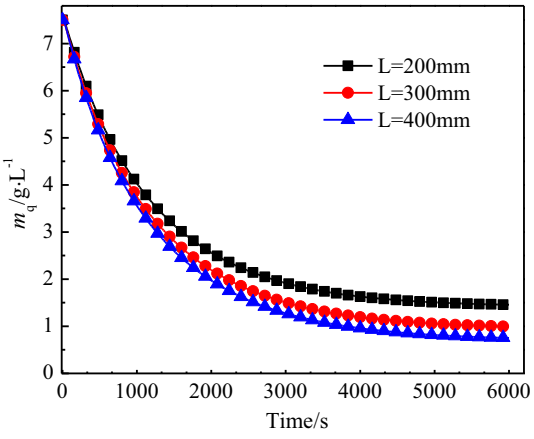

(a) Soot mass concentration

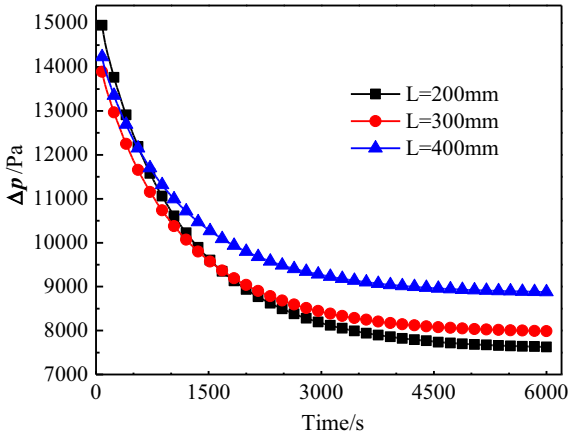

(b) Pressure drop

Fig. 6. Change trend of soot mass concentration and pressure drop in the DPFs with different length in the process of continuous regeneration (D = 266 mm, w_w = 0.31 - mm, d = 75 μm, λ_w = 10 W m^{-1} K^{-1}).

Based on the mathematical analysis above, the 3D model is built by means of software AVL Fire v2013 with the total number of cells being 655,232. The *k*-zeta-*f* model is chosen as flow model for its sufficient accuracy and stability. A detailed mechanism of 8 species and 4 relevant reactions is engaged to simulate the oxidation of soot. Semi-Implicit Method Pressure Linked Equation algorithm (SIMPLE algorithm) is employed to solve the coupled equations of pressure and velocity. As convergence criteria, the residuals for pressure is set to 5×10^{-4} Pa, the residuals for momentum is set to 5×10^{-4} kg m/s, turb.kin.rate is set to 5×10^{-4} m^2/s^3 and turb.kin. energy are set to 5×10^{-4} m^2/s^2, and the residual for energy is set to 1×10^{-4} J. Moreover, equations of momentum and continuity are discretized by central differencing scheme, and other equations are discretized by upwind scheme.

The boundary conditions of model are given as follows:

(a) For the inlet, the mass flow is applied, and fraction of species is specified by the actually measured data. Besides, the temperature is fixed.
(b) For the outlet, the pressure-outlet boundary condition is employed, where the value is set to 1×10^5 Pa, and exhaust species are simplified to sole specie, nitrogen, with value is set to 1.
(c) The standard wall function is used to dealing with thermal effect in the wall. Moreover, according to the Ref. [59], the heat transfer coefficient of the cordierite is set to 1.6 W/(m K) and the heat transfer coefficient of the SiC is set to 15.0 W/(m K).

2.2. Model verification

The test bench is composed of the diesel engine, the CR-DPF, the flowmeter, the pressure gauge, the gas analyzer (AVL AMAi60) and the electric dynamometer (Schenck DYNAS HT350) etc. Continuous regeneration of the DPF test system is shown in Fig. 3(a) and main equipments in the test bench are shown in Fig. 3(b).

The direction injection diesel engine YC4A following Chinese emission standard III is used in the experiment and its main parameters are given in Table 1, main parameters of the DOC that the cordierite is employed as the material are given in Table 2 and initial parameters for the experimental verification are given in Table 3.

The cordierite is employed as the filter material of the four DPFs (namely 1#DPF, 2#DPF, 3#DPF and 4#DPF) and the SiC is employed as the filter material of the four DPFs (namely 5#DPF, 6#DPF, 7#DPF and 8#DPF). Moreover, a test matrix of the DPF is selected as shown in Table 4.

The main test steps are expressed as follows:

- Step 1: Insulation pretreatment for the DPF

In order to get some steady and accurate experimental temperatures, insulation treatment of pipeline is done by glass wool before starting experiment.

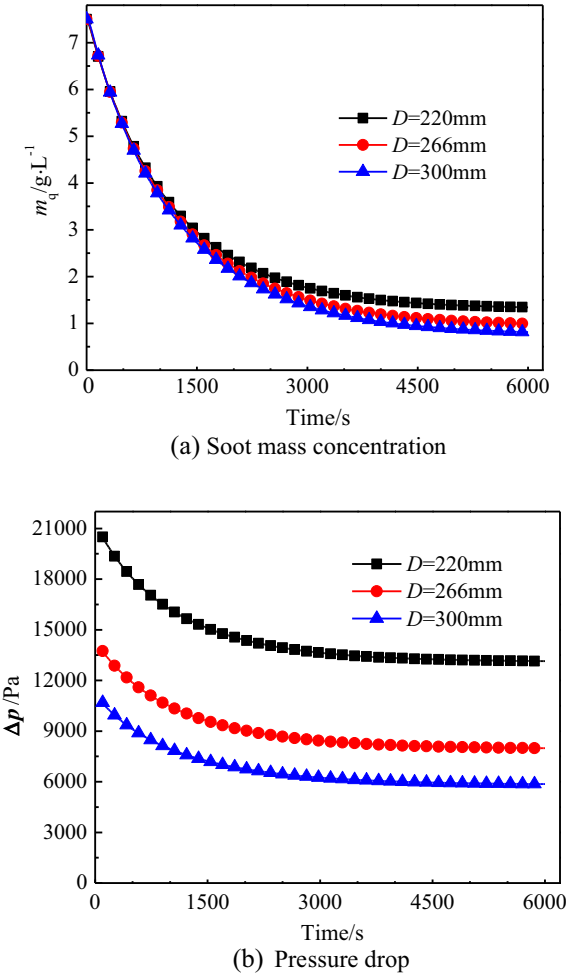

Fig. 7. Change trend of soot mass concentration and pressure drop in the DPFs with different diameter in the process of continuous regeneration (L = 300 mm, w_w = 0.31 mm, d = 75 μm, λ_w = 10 W m^{-1} K^{-1}).

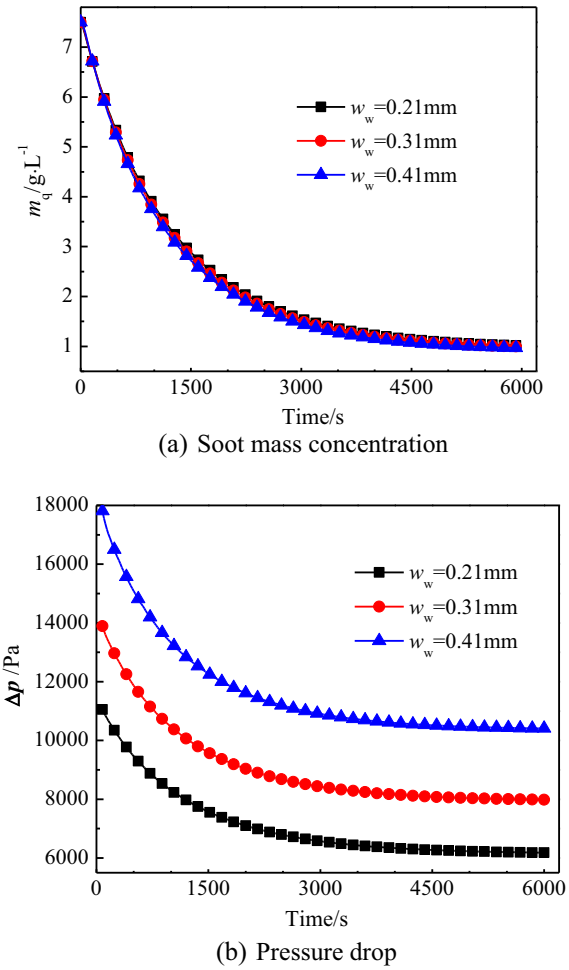

Fig. 8. Change trend of soot mass concentration and pressure drop in the DPFs with different wall thickness in the process of continuous regeneration (L = 300 mm, D = 266 mm, d = 75 μm, λ_w = 10 W m^{-1} K^{-1}).

- Step 2: Clean pretreatment for the DPF

Apart from the initial use of the new DPF, the DPF must be placed into the oven with the environmental temperature of 600 °C to bake for 10 min before each test experiment, ensuring that the residual soot deposition of the DPF is completely oxidized. Then, mass Δm_1 of the clean DPF is weighted by microgram level balance and placed on the test bench for experiments.

- Step 3: Soot capture process for the DPFs

Firstly, the valve 2 is closed and then the valve 1 is opened. When the work case of the diesel engine is stable, the valve 2 is opened firstly and then the valve 1 is closed and soot is captured by the DPFs. When the total pressure drop between inlet channel and outlet channel is kept a constant which is greater than 8.0 kPa, there occurs the phenomenon that the deposition rate of the soot is equal to the oxidation rate of the soot and the continuous regeneration "balance point" of the DPFs has happened. Therefore, the soot capture process for the DPFs is over. And then the mass Δm_2 of the DPFs with the captured soot is weighed under the temperature 150 °C by microgram level balance. And then the mass Δm_3 of the captured soot can be expressed as $\Delta m_3 = \Delta m_2 - \Delta m_1$.

As depicted in Fig. 4, let t_0 stand for the time of the soot capture process for the DPFs, then the time t_0 of the soot capture process from 1#DPF to 8#DPF is 4626 s, 4457 s, 4321 s, 4054 s, 3792 s, 3584 s, 3472 s, and 3357 s, respectively, which are shown in Table 5. The change of the key parameters such as the length of the filter, the channel diameter, wall thickness of the filter, the diameter of the filter and the thermal conductivity of the filter is an important reason resulting in different time t_0 of the process of continuous regeneration.

Fig. 5(a) depicts the comparison of pressure drop in the DPFs at the end of soot capture process by simulations and experiments. As shown in Fig. 5(a), the maximal relative error between the simulation value and measurement value from 1#DPF to 8#DPF is 1.7442%, 1.8935%, 2.2892%, 2.2086%, 2.3457%, 2.2642%, 2.3077%, and 2.4675%, respectively, displayed in Table 5, and it can be found that the max. relative error is less than 2.5%.

Fig. 5(b) depicts the mass Δm_3 of the captured soot in the DPFs at the end of soot capture process by simulations and experiments. As shown in Fig. 5(b), the maximal relative error between the simulation value and measurement value from 1#DPF to 8#DPF is 2.7650%, 2.9379%, 3.7240%, 3.3970%, 3.4152%, 2.9713%, 4.1941%, and 3.1915%, respectively, shown in Table 5, and it can be found that the max. relative error is less than 5%.

The main reason that cause the different pressure drop and soot collected reached by 1#DPF and 5#DPF is the different thermal wall conductivity. Because the different thermal wall conductivity of the DPFs causes the actual difference of the wall temperature, and different wall temperature will cause the different soot distri-

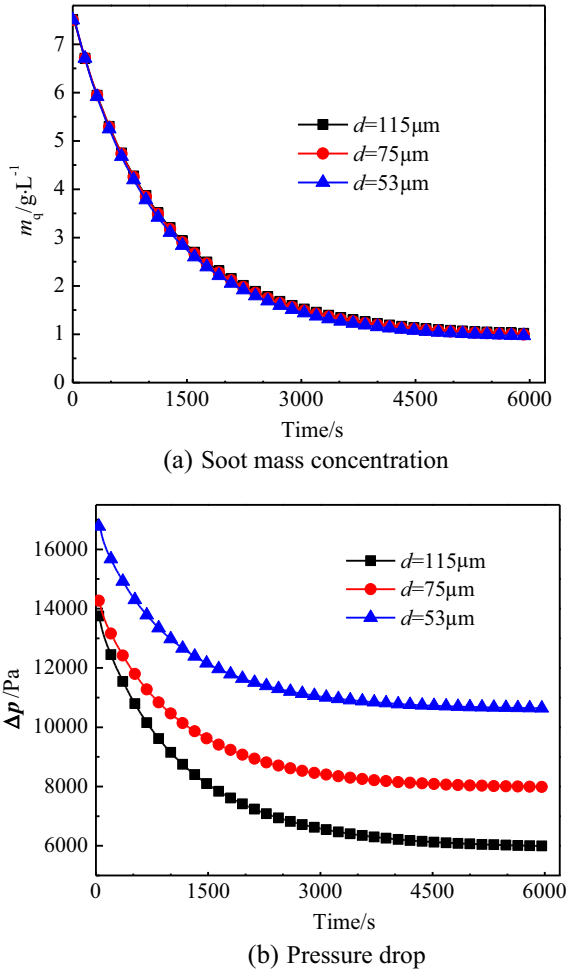

(a) Soot mass concentration

(b) Pressure drop

Fig. 9. Change trend of soot mass concentration and pressure drop in the DPFs with different channel diameter in the process of continuous regeneration (L = 300 mm, D = 266 mm, w_w = 0.31 mm, λ_w = 10 W m^{-1} K^{-1}).

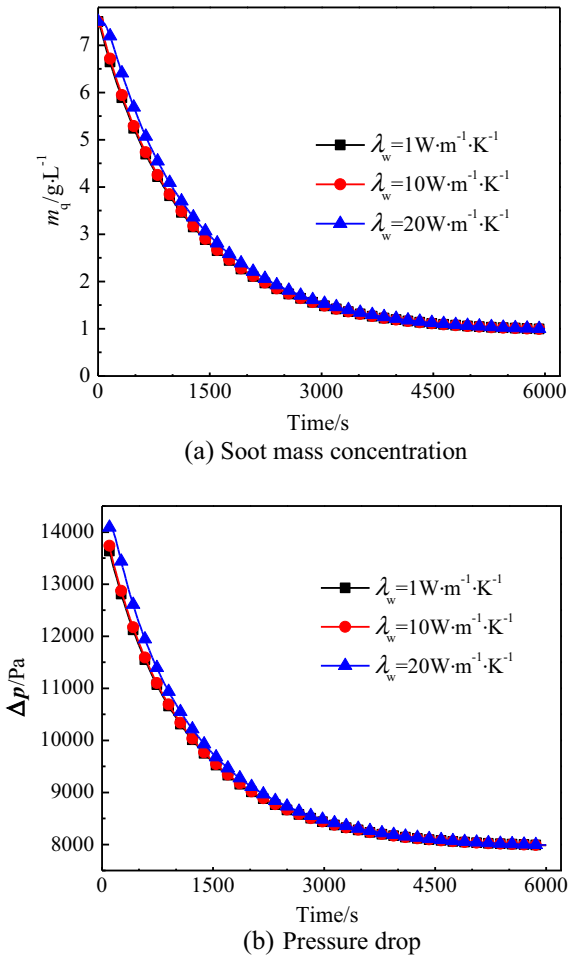

(a) Soot mass concentration

(b) Pressure drop

Fig. 10. Change trend of soot mass concentration and pressure drop in the DPFs with different heat conductivity in the process of continuous regeneration (L = 300 mm, D = 266 mm, w_w = 0.31 mm, d = 75 μm).

bution, which will lead to the different pressure drop and soot collected.

The relative error of the simulation value and measurement value of the pressure drop and the mass Δm_3 of the captured soot in the DPFs probably derives from the following reasons:

(1) The permeability k_s of soot deposition layer is treated as a constant due to nominal value of factory, but the actual permeability k_s is a random variable varying from 1.0×10^{-15} m^2 to 1.0×10^{-13} m^2 [60], which will take a greater effect on the calculation of the pressure drop and the mass Δm_3 of the captured soot. (2) The thickness δ_s of soot deposition layer is treated as a uniform thickness, and it is true that there are minute differences among thickness δ_s of soot deposition layer along the axial direction of the DPF in equilibrium state. (3) There are some unavoidable errors from measuring instrument and testing process.

Obviously, the developed simulation results of the one-dimensional mathematic model match with experimental results, which can prove that the developed mathematic model can be used to investigate the effects of key geometric parameters on equilibrium properties of continuous regeneration trap of diesel engine.

3. Results and discussion

3.1. Equilibrium characteristics of the DPFs with key parameters in the process of continuous regeneration

According to the above research results, the key parameters and their levels are determined by channel diameter d of the filter, wall thickness w_w of the filter, length L of the filter, diameter D of the DPF and thermal conductivity λ_w of the filter. All the exhaust parameters are kept in different constant, and the simulations are performed based on mass flow with 0.59 kg/s and inlet temperature at 652 K. Besides, initial soot loading with 7.5 g/L and other detailed exhaust species can be shown in Table 3.

As shown in Fig. 6, with the increase of the length of the DPF, the seepage velocities of exhaust gas across the deposition layer and the filter wall are decreased, therefore, there are more substantial reductions for soot mass concentration when the length of the DPF is increased, but there are smaller pressure drops when the length of the DPF is increased. Thus, the increase of the length of the DPF will lead to the oxidation of soot being more sufficient and accumulative temperature helping this progress. Moreover, the pressure drop of the filter is smaller when comes to equilibrium state since expansion of length largely increases the gas resistance. Besides, the decrease of soot mass concentration is not very apparent and the decrease of pressure drop is larger when the length varies from 300 to 400 mm, compared to the change from 200 to 300 mm.

For the filter length with 200 mm, there is a larger flux gas per unit area of soot cake, therefore, a larger difference of pressure drop is mainly caused by soot cake, which finally causes the different behavior of initial pressure drop, compared to the filters with length of 300 mm and 400 mm. In other words, the different filter length will cause the different soot distribution and the different soot layer will lead to the difference of initial pressure drop.

In Fig. 7, the similar trend of the reductions for soot mass concentration and the opposite trend of pressure drop can be found when the diameters of the DPF are increased, compared to the increase of length of the DPF. It is worth noting that the decrease of the diameter from 266 to 220 mm, the soot mass concentration has an appropriate increase, but sharp decreasing of pressure drop of the DPF is acquired. The results show that decrease of diameter increases the flow velocity and consequently insufficient oxidation of soot, resulting in over-high pressure drop. As a result, appropriate increase of diameter of filter can reduce exhaust back pressure to enhance engine performance.

Equilibrium properties of the DPFs with different wall thickness in the process of continuous regeneration are shown in Fig. 8. It can be found that soot mass concentration has a slight decline and pressure drop changes largely with increasing the wall thickness of the filter. That is to say, the rates of soot oxidation are not affected by the wall thickness, and thus, appropriate decrease of wall thickness can effectively reduce the pressure drop. However, rather low wall thickness will decrease the trapping efficiency, and the durability of filter should be taken into account.

Equilibrium properties of the DPFs with different channel diameter in the process of continuous regeneration are shown in Fig. 9. Obviously, the similar trend of behaviors with a slight decline of soot mass concentration and larger pressure drop can be found when decreasing the channel diameter of filter compared to increase of wall thickness. In fact, decreasing the channel diameter results in increase of cell density when diameter of the DPF and wall thickness are kept in constant, and thus specific surface area will be enlarged so that the resistance from the wall and increasing flow velocity will enhance the pressure drop of filters. Therefore, increasing channel diameter can decrease the pressure drop with slight effect to mass concentration and soot oxidation, as a result, higher channel diameter should be considered.

Fig. 10 presents equilibrium properties of the DPFs with different wall conductivity in the process of continuous regeneration. It can be found with increasing the wall conductivity, the soot mass concentration declines slowly, the same trend with the pressure drop when the soot mass concentration is higher than 1.5 g/L. And there is almost no influence on behaviors of filter when it comes to equilibrium state. Some explanations can be given that the exhaust gas temperature maintains at a higher level and heat loss per unit time is relatively small in a lower conductivity. However, higher conductivity causes the improvement of average gas

Table 6
Simulation results of equilibrium properties of the DPF based on orthogonal experimental design.

Case	d/μm	w_w/mm	L/mm	D/mm	λ_w/W m^{-1} K^{-1}	Δm_q/g	Δp/Pa	$t_{\eta 0.618}$/s
1	115	0.31	300	220	10	15.75	10234.2	1604
2	115	0.31	400	266	1	17.21	6122.6	1362
3	115	0.41	300	300	20	17.39	5299.5	1526
4	75	0.21	300	266	10	16.86	6182.2	1508
5	75	0.31	300	300	1	17.21	5855.8	1393
6	75	0.31	300	300	20	17.33	5859.9	1529
7	75	0.41	200	266	10	15.78	9827.4	1625
8	75	0.41	400	266	10	16.16	11590.9	1282
9	75	0.41	300	300	20	16.95	7663.0	1518
10	53	0.31	200	266	1	15.89	9305.1	1664
11	53	0.31	300	300	10	17.33	7926.7	1529
12	53	0.41	300	300	20	16.33	10956.2	1475

temperature, and thus the pressure drop is enhanced. And small difference of average gas temperature is formed when in an equilibrium state.

3.2. Fuzzy grey relational analysis on effects of key parameters on equilibrium properties of the DPF in the process of continuous regeneration

Grey Relational Analysis (GRA) is a way of measuring the degree of correlation between different factors based on similar or dissimilar degree of development trend [61,62]. It is developed to reveal the inherent regularity between various factors without strict restrictions, and has been applied to a wide range of fields [63–65]. In this paper, the GRA is employed to make a weight analysis of impact of various factors on equilibrium mass, pressure drop and regeneration rate. Here are the procedures:

(1) Establish the comparison matrix and reference matrix. The comparison matrix $\boldsymbol{X}'$ can be described as follow:

$$\mathbf{X}' = \begin{bmatrix} x'_1 \\ x'_2 \\ \vdots \\ x'_m \end{bmatrix} = \begin{bmatrix} x'_1(1) & x'_1(2) & \cdots & x'_1(n) \\ x'_2(1) & x'_2(2) & \cdots & x'_2(n) \\ \vdots & \vdots & \vdots & \vdots \\ x'_m(1) & x'_m(2) & \cdots & x'_m(n) \end{bmatrix} \tag{27}$$

where m presents the total number of factors, n presents various conditions.

And reference matrix $\boldsymbol{Y}$ can be expressed as follows:

$$Y = \begin{bmatrix} y_1(1) & y_1(2) & \cdots & y_1(n) \\ y_2(1) & y_2(2) & \cdots & y_2(n) \\ \vdots & \vdots & \vdots & \vdots \\ y_p(1) & y_p(2) & \cdots & y_p(n) \end{bmatrix} \tag{28}$$

where p presents the total number of reference targets.

(2) Nondimensionalize data of factors.

Data have various dimensions, and they can be nondimensionalized as follows:

$$x_i(k) = \frac{x'_i(k) - \min x'_i}{\max x'_i - \min x'_i} \tag{29}$$

And finally $\boldsymbol{X}'$ becomes $\boldsymbol{X}$, it can be displayed as follows:

$$X = \begin{bmatrix} x_1 \\ x_2 \\ \vdots \\ x_m \end{bmatrix} = \begin{bmatrix} x_1(1) & x_1(2) & \cdots & x_1(n) \\ x_2(1) & x_2(2) & \cdots & x_2(n) \\ \vdots & \vdots & \vdots & \vdots \\ x_m(1) & x_m(2) & \cdots & x_m(n) \end{bmatrix} \tag{30}$$

(3) Compute the cosine value of fuzzy factors. And the cosine value reflects the similarity of two factors.

$$r_{1-ij} = \frac{\Sigma_{k=1}^{n} y_j(k) x_i(k)}{\sqrt{\Sigma_{k=1}^{n} y_j(k)^2} \sqrt{\Sigma_{k=1}^{n} x_i(k)^2}}, (i = 1, 2, \ldots, m; j = 1, 2, \ldots, p) \tag{31}$$

(4) Compute the correlation coefficient.

$$\xi_{ij} = \frac{\Delta_{\min ij} + l\Delta_{\max ij}}{\Delta(k) + l\Delta_{\max ij}} \tag{32}$$

where $\Delta_{\min\ ij}$ and $\Delta_{\max\ ij}$ can be calculated as follows:

$$\Delta_{\min ij} = \min |y_j(k) - x_i(k)| (i = 1, 2, \ldots, m; j = 1, 2, \ldots, p), \tag{33}$$

$$\Delta_{\max ij} = \max |y_j(k) - x_i(k)| (i = 1, 2, \ldots, m; j = 1, 2, \ldots, p), \tag{34}$$

$$\Delta(k) = |y_j(k) - x_i(k)| (i = 1, 2, \ldots, m; j = 1, 2, \ldots, p), \tag{35}$$

(5) Define the weight vector of various factors, which applies Fuzzy Mathematics of Euclidean distance to improve the accuracy.

$$w = (w_1, w_2, \ldots, w_m) \tag{36}$$

And then compute the Euclidean coefficient:

$$r_{2-ij} = 1 - 2\sqrt{\Sigma_{j=1}^{n} \left[w_i (1 - \xi_{ij}) \right]^2} \tag{37}$$

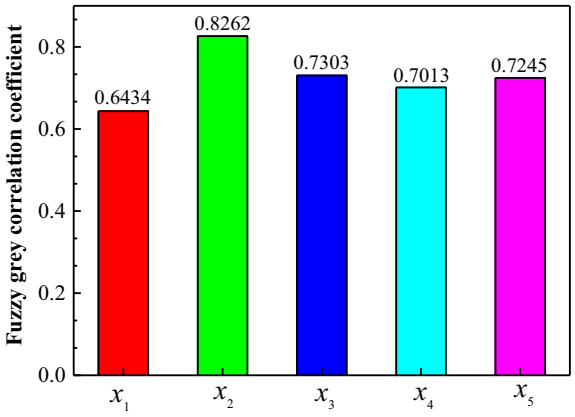

(a) Soot mass in the DPF in equilibrium state

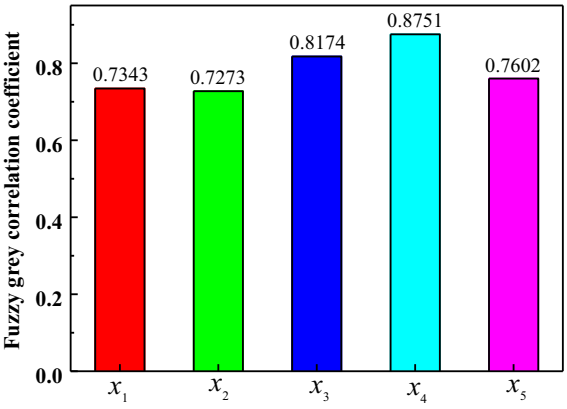

(b) Pressure drop in the DPF in equilibrium state

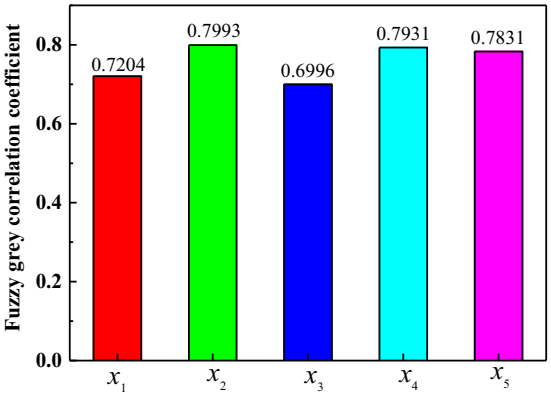

(c) Oxidation rate in the DPF in equilibrium state

Fig. 11. Fuzzy grey correlation coefficient of different effect factors on equilibrium properties of the DPF in equilibrium state.

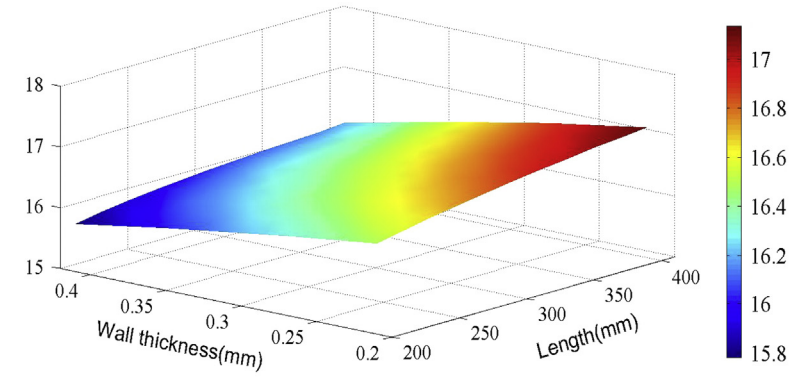

(a) Change laws of the soot mass in the DPF based on different wall thicknesses and lengths

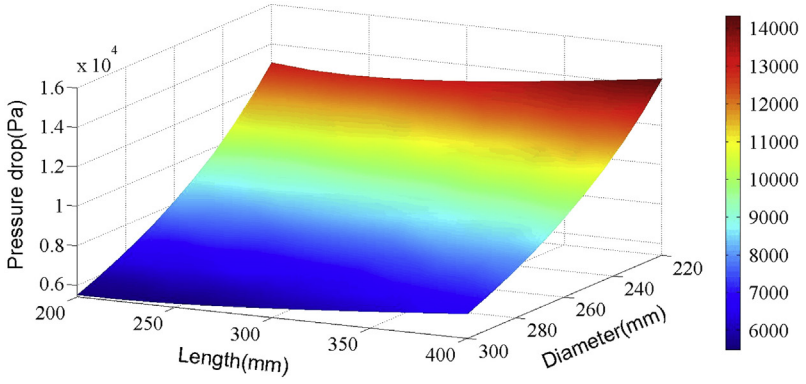

(b) Change laws of pressure drop in the DPF based on different diameters and lengths

Fig. 12. Change laws of soot mass and pressure drop in the DPF in equilibrium state based on different geometric parameters.

(6) Finally, the fuzzy grey correlation coefficient can be calculated based on what is discussed above, which can be expressed as follows:

$$r_{ij} = \sqrt{\frac{r_{1-ij}^2 + r_{2-ij}^2}{2}} \tag{38}$$

With the help of the orthogonal distribution of the key parameters, the simulation of testing cases is acquired shown in Table 6. It is obvious that the equilibrium mass, pressure drop and oxidation rate are affected differently by various structural parameters from Table 4 and the results are shown above. Moreover, the time $t_{\eta 0.618}$ of regeneration efficiency coming to 61.8% is applied as a reference index to reflect the oxidation rate.

Let five effect factors (such as channel diameter of the filter, wall thickness of the filter, length of the filter, diameter of the DPF and thermal conductivity of the filter) as comparison factors, i.e., $x_1(k)$, $x_2(k)$, $x_3(k)$, $x_4(k)$, and $x_5(k)$, and let soot mass in the DPF in regeneration equilibrium state, pressure drop in the DPF in regeneration equilibrium state and oxidation rate ($t_{\eta 0.618}$) as reference targets. The reference matrix and comparison matrix are expressed as follows:

$$X = \begin{bmatrix} 125 & 125 & 125 & 200 & 200 & 200 & 200 & 200 & 200 & 275 & 275 & 275 \\ 0.31 & 0.31 & 0.41 & 0.21 & 0.31 & 0.31 & 0.41 & 0.41 & 0.41 & 0.31 & 0.31 & 0.41 \\ 300 & 400 & 300 & 300 & 300 & 300 & 200 & 400 & 300 & 200 & 300 & 300 \\ 220 & 266 & 300 & 266 & 300 & 300 & 266 & 266 & 300 & 266 & 300 & 300 \\ 10 & 1 & 100 & 10 & 1 & 100 & 10 & 10 & 100 & 1 & 10 & 100 \end{bmatrix}$$

$$Y = \begin{bmatrix} 15.75 & 17.21 & 17.39 & 16.86 & 17.21 & 17.33 & 15.78 & 16.16 & 16.95 & 15.89 & 17.33 & 16.33 \\ 10234 & 6124 & 5299 & 6182 & 5859 & 5860 & 9827 & 11591 & 7663 & 9305 & 7927 & 10956 \\ 1604 & 1362 & 1526 & 1508 & 1393 & 1529 & 1625 & 1282 & 1518 & 1664 & 1529 & 1475 \end{bmatrix}$$

As shown in Fig. 11, the fuzzy grey correlation coefficient can be calculated by Eq. (27)–(38), and the calculation results are expressed as follows: (a) the fuzzy grey correlation coefficients of five effect factors on the soot mass in the DPF in equilibrium state are 0.6434, 0.8262, 0.7303, 0.7013, 0.7245, therefore, the soot mass in the DPF in equilibrium state are more under the influence of wall thickness of the filter, but are less under the influence of channel diameter of the filter; (b) the fuzzy grey correlation coefficients of five effect factors on the pressure drop in the DPF in equilibrium state 0.7343, 0.7273, 0.8174, 0.8751, 0.7602, therefore, the diameter of the DPF exerts much influence on the pressure drop in the DPF in equilibrium state, but the wall thickness of the filter exerts little influence on it; (c) the fuzzy grey correlation coefficients of five effect factors on the oxidation rate are 0.7204, 0.7993, 0.6996, 0.7931, 0.7831, therefore, the oxidation rate are more influenced by the wall thickness of the filter and are less influenced by the length of the filter.

The key parameters affect soot mass and pressure drop in the DPF in equilibrium state and their change laws is shown in Fig. 12. Although the correlation factor for wall thickness is the highest affecting soot mass, it is only marginally higher than those for other factors. With the increase of wall thickness of the filter and channel diameter of the filter in equilibrium state, soot mass in the DPF in equilibrium state will be reduced obviously. But for variation of pressure drop in the DPF in equilibrium state, it is more complicated as follows: (a) when the diameter of the filter is about 300 mm, pressure drop in the DPF in equilibrium state will raise with increase of the length of filter; (b) when the diameter of the filter is about 220 mm, pressure drop in the DPF in equilibrium state will cut down firstly and then raise with increase of the length of the filter. Besides, the optimum length of the filter may not necessarily be the smallest possible, sometimes depending on diameter of the filter. And smaller diameter of the DPF results in larger pressure drop in the DPF in equilibrium state.

4. Conclusions

(1) A bigger wall thickness can greatly increase the back pressure of the filter when regeneration comes to an equilibrium state, and a thinner thickness should be considered if trapping efficiency and service lifetime can meet the requirements.
(2) The less soot mass concentration in the DPF in equilibrium state can be acquired if diameter of the filter is appropriately increased, excess soot mass in the DPF in equilibrium state will cause some bad influences such as soot substances forming easily into lumps, their oxidation being more difficult, channels being easily plugged and finally will lead to the regeneration of the DPF being deteriorated.
(3) The soot mass in the DPF in equilibrium state are more under the influence of wall thickness of the filter, and the diameter of the DPF exerts much influence on the pressure drop in the DPF in equilibrium state, the oxidation rate are more influenced by the wall thickness of the filter. However, it is worth pointing out that although the correlation factor for wall thickness is the highest affecting soot mass, it is only marginally higher than those for other factors.
(4) Smaller diameter of the DPF will result in larger pressure drop in the DPF and more complications for the length of the filter in equilibrium state. The optimum length of the filter may not necessarily be the smallest possible, sometimes depending on diameter of the filter in equilibrium state. Besides, ash-loaded DPFs may make pressure drop more unpredictable, but and this article doesn't discuss about it detailedly.

Conflict of interests

The authors declare that they have no conflict of interests regarding the publication of this paper.

Acknowledgements

This work is supported by the National Natural Science Foundation of China under the research grant of 51676066 and 51606162 and the China Scholarship Council under the research grant of 201606130020.

References

[1] J. Li, W.M. Yang, H. An, D. Zhao, Effects of fuel ratio and injection timing on gasoline/biodiesel fueled RCCI engine: a modeling study, Appl. Energy 155 (2015) 59–67.
[2] H. An, W.M. Yang, J. Li, D.Z. Zhou, Modeling study of oxygenated fuels on diesel combustion: effects of oxygen concentration, cetane number and C/H ratio, Energy Convers. Manage. 90 (2015) 261–271.
[3] J. Benajes, S. Molina, A. García, J. Monsalve-Serrano, R. Durrett, Performance and engine-out emissions evaluation of the double injection strategy applied to the gasoline partially premixed compression ignition spark assisted combustion concept, Appl. Energy 134 (2014) 90–101.
[4] J. Benajes, A. García, V. Domenech, R. Durrett, An investigation of partially premixed compression ignition combustion using gasoline and spark assistance, Appl. Therm. Eng. 52 (2) (2013) 468–477.
[5] J. Benajes, S. Molina, A. García, J. Monsalve-Serrano, Effects of low reactivity fuel characteristics and blending ratio on low load RCCI (reactivity controlled compression ignition) performance and emissions in a heavy-duty diesel engine, Energy 90 (2015) 1261–1271.
[6] A. Paykani, A.H. Kakaee, P. Rahnama, R.D. Reitz, Effects of diesel injection strategy on natural gas/diesel reactivity controlled compression ignition combustion, Energy 90 (2015) 814–826.
[7] S. Dev, P. Divekar, K. Xie, X. Han, X. Chen, M. Zheng, A study of combustion inefficiency in diesel LTC and gasoline-diesel RCCI via detailed emission measurement, J. Eng. Gas Turbines Power 137(12) (2015) 121501–121501-7.
[8] D.Z. Zhou, W.M. Yang, H. An, J. Li, Application of CFD-chemical kinetics approach in detecting RCCI engine knocking fuelled with biodiesel/methanol, Appl. Energy 145 (2015) 255–264.
[9] M. Zheng, X. Han, U. Asad, J. Wang, Investigation of butanol-fuelled HCCI combustion on a high efficiency diesel engine, Energy Convers. Manage. 98 (2015) 215–224.
[10] G.T. Reader, U. Asad, M. Zheng, Energy efficiency trade-off with phasing of HCCI combustion, Int. J. Energy Res. 37 (3) (2013) 200–210.
[11] D. Zhao, Waste thermal energy harvesting from a convection-driven Rijke-Zhao thermo-acoustic-piezo system, Energy Convers. Manage. 66 (2013) 87–97.
[12] D. Zhao, E. Ega, Energy harvesting from self-sustained aeroelastic limit cycle oscillations of rectangular wings, Appl. Phys. Lett. 105 (2014) 103903.
[13] D. Zhao, J.W. Li, Feedback control of combustion instabilities using a Helmholtz resonator with an oscillating volume, Combust. Sci. Technol. 104 (2012) 694–716.
[14] D. Zhao, Transient growth of flow disturbances in triggering a Rijke tube combustion instability, Combust. Flame 159 (2012) 2126–2137.
[15] C. Benaqqa, M. Gomina, A. Beurotte, M. Boussuge, B. Delattre, K. Pajot, E. Pawlak, F. Rodrigues, Morphology, physical, thermal and mechanical properties of the constitutive materials of diesel particulate filters, Appl. Therm. Eng. 62 (2) (2014) 599–606.
[16] D. Buono, A. Senatore, M.V. Prati, Particulate filter behaviour of a Diesel engine fueled with biodiesel, Appl. Therm. Eng. 49 (2012) 147–153.
[17] J.H. Jiang, J.K. Gong, W.Q. Liu, T. Chen, C. Zhong, Analysis on filtration characteristic of wall-flow filter for ash deposition in cake, J. Aerosol Sci. 95 (2016) 73–83.
[18] B. Zhang, J.K. Gong, J.Q. E, Y. Li, Failure recognition of the diesel particulate filter based on catastrophe theory, Can. J. Chem. Eng. 94(3) (2016) 596–602.
[19] B. Guan, R. Zhan, H. Lin, Z. Huang, Review of the state-of-the-art of exhaust particulate filter technology in internal combustion engines, J. Environ. Manage. 154 (2015) 225–258.
[20] X. Zhang, D.O. Hayward, D.M.P. Mingos, Effects of microwave dielectric heating on heterogeneous catalysis, Catal. Lett. 88 (2003) 1–2.
[21] V. Palma, P. Ciambelli, E. Meloni, A. Sin, Catalytic DPF microwave assisted active regeneration, Fuel 140 (2015) 50–61.
[22] V. Palma, E. Meloni, Microwave assisted regeneration of a catalytic diesel soot trap, Fuel 181 (2016) 421–429.
[23] V. Palma, P. Ciambelli, E. Meloni, A. Sin, Study of the catalyst load for a microwave susceptible catalytic DPF, Catal. Today 216 (2013) 185–193.
[24] J.Q. E, W. Zuo, J.X. Gao, Q.G. Peng, Z.Q. Zhang, P.M. Hieu, Effect analysis on pressure drop of the continuous regeneration-diesel particulate filter based on NO_2 assisted regeneration, Appl. Therm. Eng. 100 (2016) 356–366.

[25] J.Q. E, L.F. Xie, Q.S. Zuo, G.J. Zhang, Effect analysis on regeneration speed of continuous regeneration-diesel particulate filter based on NO_2-assisted regeneration, Atmos. Pollut. Res. 7(1) (2016) 9–17.
[26] S.J. Lee, S.J. Jeong, W.S. Kim, Computational study on the effects of volume ratio of DOC/DPF and catalyst loading on the PM and NO_x emission control for heavy-duty diesel engines, Int. J. Automot. Technol. 9 (6) (2008) 659–670.
[27] R. Allanson, P. Blakeman, B. Cooper, Optimising the low temperature performance and regeneration efficiency of the continuously regenerating diesel particulate filter (CR-DPF) system, SAE 2002-01-0428.
[28] B. Zhang, J.Q. E, J.K. Gong, W.H. Yuan, W. Zuo, Y. Li, J. Fu, Multidisciplinary design optimization of the diesel particulate filter in the composite regeneration process, Appl. Energy 181 (2016) 14–28.
[29] J.Q. E, M. Liu, Y.W. Deng, H. Zhu, J.K. Gong, Influence analysis of monolith structure on regeneration temperature in the process of microwave regeneration in the diesel particulate filter, Can. J. Chem. Eng. 94(1) (2016) 168–174.
[30] Q.S. Zuo, D.M. Zhang, J.Q. E, J.K. Gong, Comprehensive analysis on influencing factors of composite regeneration performance of a diesel particulate filter, Environ. Prog. Sustain. Energy 35(3) (2016) 882–890.
[31] J.Q. E, Q.S. Zuo, H.L. Liu, Y. Li, J.K. Gong, Endpoint forecasting on composite regeneration by coupling cerium-based additive and microwave for diesel particulate filter, J. Cent. South Univ. 23(8) (2016) 2118–2128.
[32] M. Schejbal, J. Štěpánek, M. Marek, P. Kočí, M. Kubíček, Modelling of soot oxidation by NO_2 in various types of diesel particulate filters, Fuel 89 (9) (2010) 2365–2375.
[33] D. Fino, S. Bensaid, M. Piumetti, N. Russo, A review on the catalytic combustion of soot in diesel particulate filters for automotive applications: from powder catalysts to structured reactors, Appl. Catal. A 509 (2016) 75–96.
[34] C.J. Tighe, M.V. Twigg, A.N. Hayhurst, J.S. Dennis, The kinetics of oxidation of diesel soots by NO_2, Combust. Flame 159 (2012) 77–90.
[35] F. Piscaglia, G. Ferrari, A novel 1D approach for the simulation of unsteady reacting flows in diesel exhaust after-treatment systems, Energy 34 (2009) 2051–2062.
[36] A.J. Torregrosa, J.R. Serrano, F.J. Arnau, P. Piqueras, A fluid dynamic model for unsteady compressible flow in wall-flow diesel particulate filters, Energy 36 (1) (2011) 671–684.
[37] I.P. Kandylas, G.C. Koltsakis, A.M. Stamatelos, Mathematical modeling of precious metals catalytic converters for diesel NO_x reduction, Proc. Inst. Mech. Eng. Part D J. Automob. Eng. 213 (3) (1999) 279–292.
[38] I.P. Kandylas, G.C. Koltsakis, NO_2-assisted regeneration of diesel particulate filters: a modeling study, Ind. Eng. Chem. Res. 41 (9) (2002) 2115–2123.
[39] A.G. Konstandopoulos, Fundamental studies of diesel particulate filters: transient loading, regeneration and aging. SAE Paper 2000-01-1016.2000.
[40] T. Tang, J. Zhang, D.X. Cao, S.J. Shuai, Y.G. Zhao, Experimental study on filtration and continuous regeneration of a particulate filter system for heavy-duty diesel engines, J. Environ. Sci. 26 (12) (2014) 2434–2439.
[41] S.Z. Bai, J. Tang, G.H. Wang, G.X. Li, Soot loading estimation model and passive regeneration characteristics of DPF system for heavy-duty engine, Appl. Therm. Eng. 100 (2016) 1292–1298.
[42] F. Payri, A. Broatch, J.R. Serrano, P. Piqueras, Experimental–theoretical methodology for determination of inertial pressure drop distribution and pore structure properties in wall-flow diesel particulate filters (DPFs), Energy 36 (2011) 6731–6744.
[43] S.J. Lee, S.J. Jeong, W.S. Kim, Numerical design of the diesel particulate filter for optimum thermal performances during regeneration, Appl. Energy 86 (2009) 1124–1135.
[44] J. Rodríguez-Fernández, F. Oliva, R.A. Vázquez, Characterization of the diesel soot oxidation process through an optimized thermogravimetric method, Energy Fuel 25 (2011) 2039–2048.
[45] I.P. Kandylas, O.A. Haralampous, G.C. Koltsakis, Diesel soot oxidation with NO_2: engine experiments and simulations, Ind. Eng. Chem. Res. 41 (2002) 5372–5384.
[46] B. Peters, A. Dziugys, Numerical modeling of electrified particle layer formation on the surface of filtration fabric, Environ. Eng. 9 (4) (2001) 191–197.
[47] B. Peters, A. Dziugys, Numerical simulation of the motion of granular material using object-oriented techniques, Comput. Methods Appl. Mech. Eng. 191 (2002) 1983–2001.
[48] Z.H. Shon, K.H. Kim, S.K. Song, Long-term trend in NO_2 and NO_x levels and their emission ratio in relation to road traffic activities in East Asia, Atmos. Environ. 45 (2011) 3120–3131.
[49] J.P.A. Neeft, T.X. Nijhuis, E. Smakman, Kinetics of the oxidation of diesel soot, Fuel 76 (12) (1997) 1129–1136.
[50] A.G. Konstandopoulos, Fundamental studies of diesel particulate filters: transient loading, regeneration and aging, SAE Paper 2000-01-1016.
[51] G.C. Koltsakis, A.M. Stamatelos, Modeling catalytic regeneration of wall-flow particulate filters, Ind. Eng. Chem. Res. 35 (1996) 2–13.
[52] K.N. Pattas, A.M. Stamatelos, K.N. Kougianos, Trap protection by limiting A/F ratio during regeneration, SAE: Warrendale, PA, 1995, 950366.
[53] A.Y. Stakheev, A.M. Gololobov, G.N. Baeva, G.O. Bragina, N.S. Telegina, Oxidation of soot with $NO+O_2$ over Pt catalyst: direct evaluation of Pt catalyst efficiency in NO to NO_2 recycling, Mendeleev Commun. 20 (2010) 269–270.
[54] H. Burtscher, Physical characterization of particulate emissions from diesel engines: a review, J. Aerosol Sci. 36 (2005) 896–932.
[55] A.G. Konstandopoulos, M. Kostoglou, Reciprocating flow regeneration of soot filters, Combust. Flame 121 (2000) 488–500.
[56] A.G. Konstandopoulos, J.H. Johnson, Wall-flow diesel particulate filters-their pressure drop and collection efficiency, SAE technical, 1989, 890405.
[57] F. Millo, M. Andreata, M. Rafigh, D. Mercuri, C. Pozzi, Impact on vehicle fuel economy of the soot loading on diesel particulate filters made of different substrate materials, Energy 86 (2015) 19–30.
[58] A.K. Agarwal, Biofuels (alcohols and biodiesel) applications as fuels for internal combustion engines, Prog. Energy Combust. Sci. 33 (2007) 233–271.
[59] Y. Miyairi, S. Miwa, F. Abe, Z. Xu, Y. Nakasuji, Numerical study on forced regeneration of wall-flow diesel particulate filter, SAE Technical Paper 2001-01-0912.
[60] A.G. Konstandopoulos, Inertial contributions to the pressure drop of diesel particulate filters, SAE Technical Paper 2001-01-0909.
[61] G. Taguchi, Introduction to quality engineering: designing quality into products and processes, ARRB Group Limited, 1986.
[62] J.Q. E, Y.Q. Li, J.K. Gong, Function chain neural network prediction on heat transfer performance of oscillating heat pipe based on grey relational analysis, J. Cent. South Univ. Technol. 18(5) (2011) 1733–1737.
[63] A. Kadier, P. Abdeshahian, Y. Simayi, Grey relational analysis for comparative assessment of different cathode materials in microbial electrolysis cells, Energy 90 (2015) 1556–1562.
[64] Z. Wang, T. Lei, X. Chang, X. Shi, J. Xiao, Optimization of a biomass briquette fuel system based on grey relational analysis and analytic hierarchy process: a study using cornstalks in China, Appl. Energy 157 (2015) 523–532.
[65] W. Zuo, J.Q. E, X.L. Liu, Q.G. Peng, Y.W. Deng, H. Zhu, Orthogonal experimental design and fuzzy grey relational analysis for emitter efficiency of the micro-cylindrical combustor with a step, Appl. Therm. Eng. 103 (2016) 945–951.